

GA-A23366

**RUNAWAY ELECTRON PRODUCTION
IN DIII-D KILLER PELLET EXPERIMENTS,
CALCULATED WITH THE CQL3D/KPRAD MODEL**

by

**R.W. HARVEY, V.S. CHAN, S.C. CHIU, T.E. EVANS,
M.N. ROSENBLUTH, and D.G. WHYTE**

MAY 2000

DISCLAIMER

This report was prepared as an account of work sponsored by an agency of the United States Government. Neither the United States Government nor any agency thereof, nor any of their employees, makes any warranty, express or implied, or assumes any legal liability or responsibility for the accuracy, completeness, or usefulness of any information, apparatus, product, or process disclosed, or represents that its use would not infringe privately owned rights. Reference herein to any specific commercial product, process, or service by trade name, trademark, manufacturer, or otherwise, does not necessarily constitute or imply its endorsement, recommendation, or favoring by the United States Government or any agency thereof. The views and opinions of authors expressed herein do not necessarily state or reflect those of the United States Government or any agency thereof.

**RUNAWAY ELECTRON PRODUCTION
IN DIII-D KILLER PELLET EXPERIMENTS,
CALCULATED WITH THE CQL3D/KPRAD MODEL**

by

**R.W. HARVEY,* V.S. CHAN, S.C. CHIU,† T.E. EVANS,
M.N. ROSENBLUTH, and D.G. WHYTE‡**

This is a preprint of a paper submitted for publication in
Phys. Plasmas.

*CompX, Del Mar, California 92014-5672.

†Sunrise R&M, Inc., San Diego, California.

‡University of California at San Diego, La Jolla, California 92093-0417.

**Work supported by
the U.S. Department of Energy
under Contract No. DE-AC03-99ER54463
and Grant No. DE-FG03-99ER54541**

**GA PROJECT 03726
MAY 2000**

ABSTRACT

Runaway electrons are calculated to be produced during the rapid plasma cooling resulting from “killer pellet” injection experiments, in general agreement with observations in the DIII-D tokamak. The time-dependent dynamics of the kinetic runaway distributions are obtained with the CQL3D collisional Fokker-Planck code, including the effect of small and large angle collisions and stochastic magnetic field transport losses. The background density, temperature and Z_{eff} are evolved according to the KPRAD deposition and radiation model of pellet-plasma interactions. Three distinct runaway mechanisms are apparent: (1) prompt “hot-tail runaways” due to the residual hot electron tail remaining from the pre-cooling phase, (2) “knock-on” runaways produced by large-angle Coulomb collisions on existing high energy electrons, and (3) Dreicer “drizzle” runaway electrons due to diffusion of electrons up to the critical velocity for electron runaway. For electron densities below $\approx 1 \cdot 10^{15} \text{ cm}^{-3}$, the hot-tail runaways dominate the early time evolution, and provide the seed population for late time knock-on runaway avalanche. For small enough stochastic magnetic field transport losses, the knock-on production of electrons balances the losses at late times. For losses due to radial magnetic field perturbations in excess of $\approx 0.1\%$ of the background field, i.e., $\delta B_r/B \geq 0.001$, the losses prevent late-time electron runaway.

1 Introduction

Disruptions in large tokamaks can lead to conversion of the plasma current to runaway electron current. The disruptions are accompanied by a vertical instability of the plasma resulting in scrape-off of the plasma and runaways on the surrounding components. As a result, the plasma facing components may be damaged [1, 2, 3]. To mitigate these problems it has been proposed that “killer pellets” be preemptively injected into the plasma to radiatively cool the plasma and give a controlled shutdown. In either case of disruption or pellet injection, the plasma cools on a time scale short compared to the plasma resistive time in the machine and consequently the current is reasonably constant during this “thermal quench” stage. The electric field therefore increases $\propto Z_{\text{eff}} T_e^{-3/2}$ as the temperature drops. In the resulting large electric field, the electrons can runaway to large energies by three distinct mechanisms: (1) prompt “hot-tail runaways” due to the residual hot electron tail remaining from the pre-cooling phase occurring when the slowing down time for three electrons is longer than the cooling time [4], (2) “knock-on” runaways produced by large-angle Coulomb collisions or existing high energy electrons [5, 6], and (3) Dreicer “drizzle” runaway electrons due to diffusion of electrons up to the runaway velocity [7]. The “hot-tail runaways” are emphasized in this report; we will address primarily DIII-D “killer-pellet” experimental conditions although the results have wider applicability. It is found that essentially full conversion of the plasma current to runaway current is promptly obtained, for densities such that the slowing down time of the tail electrons at three times the thermal velocity $v_{te} = \sqrt{T_e/m_e}$ is greater than the plasma cooling time down to 10 eV. The “hot-tail runaway” is essentially a dynamical process in which substantial numbers of electrons remain above the critical velocity for runaway in the large electric field immediately after the temperature drop. The electric field subsequently decreases due to the increase in electrical conductivity resulting from the runaways. If losses are included in the analysis, then the runaways will accordingly disappear, except that they may be sustained by the large-angle scattering “knock-on”

process. In the DIII-D “killer pellet” scenarios, the Dreicer “drizzle” process is not a significant source of runaway electrons.

The present paper uses the CQL3D bounce-averaged Fokker-Planck code[8] to model the time-dependence (*i.e.*, dynamics) of formation of runaway distributions at several radii within the plasma. CQL3D calculates the distribution functions of electrons as a function of momentum parallel, u_{\parallel} , and perpendicular, u_{\perp} , to the ambient magnetic field. The gyromotion and the particle bounce motion in toroidal geometry in the full six-dimensional Fokker-Planck equation have been averaged over, based on the assumption that the time-scales for these processes are short compared to the time-scales of interest. Toroidal symmetry is assumed. The neoclassical radial drifts of the particles are neglected giving the “zero-banana-width” approximation. This gives a three dimensional ($u_{\parallel}, u_{\perp}, \rho$) time-dependent equation to solve for the electron distributions [9, 10]. The code uses a relativistic generalization [11] of the full nonlinear collision operator [12]. A knock-on collision operator has been added to the code as described in Ref. [4], and more completely in the following section. A new addition for the present work is a model of stochastic magnetic field losses following evidence from tokamaks that this is a key component of the physics in pellet injection experiments [13, 14].

We solve the Fokker-Planck equation with CQL3D flux-surface by flux-surface, and rely upon the KPRAD pellet deposition and radiation loss code [15] to provide the evolution of the bulk properties (density, temperature and Z_{eff}) of the plasma. Tail electron losses are modeled using a simple loss-time operator which causes electrons to be removed at a given velocity-dependent rate. The periods of plasma evolution we consider are short compared to the resistive time, and therefore we calculate the electric field according to the condition that the local current density, including the nonthermal electrons, is constant.

In the following sections, we describe the relevant CQL3D features including implementation of the “knock-on” operator and the stochastic magnetic field losses. Frequently [16]

the thermal portion of the plasma in the low temperature phase of evolution after the thermal quench is no longer in the neoclassical banana regime, that is, for the low temperature phase the collision time τ_e becomes less than the bounce time τ_b . In this case, the contribution to the plasma current from the low velocity electrons must be calculated from the neoclassical formulas [17].

A simulation based on a Ne pellet injection scenario in DIII-D [18] is presented in detail. This is an intermediate case in that the hot-tail runaway, the knock-on runaway production, and the losses all play an important role in the simulation. A temperature drop from 2.2 keV to 10 eV in 0.1 ms at plasma radius 0.6a gives prompt conversion of 0.6 of the plasma current to runaway current, and, in the absence of losses, this fraction rapidly exponentiates to 100 percent due to the knock-on process. With losses due to stochastic radial magnetic field $\delta B_r/B = 0.001$, the runaway current fraction due to the balance between knock-on runaway production and the losses settles back to 0.2 of the plasma current. Parameter variations were conducted around this fiducial simulation.

The build-up of runaway electrons does not occur for $\delta B_r/B$ greater than 0.15% at $r/a = 0.6$, or $\delta B_r/B$ greater than 0.02% at $r/a = 0.9$. If the temperature-drop-time is reduced [using a linear relationship between $\log(T_e)$ and $\log(t)$], then the amount of $\delta B_r/B$ -losses required to suppress runaway conversion increases in a manner that will be described. The hot-tail runaway electrons lead to prompt conversion of plasma current to runaway current and/or provide the major seed population for knock-on avalanche for plasma densities below $\sim 10^{15} \text{ cm}^{-3}$. At higher densities the tail slowing-down-time becomes short compared to the temperature-drop-time reducing the hot-tail fraction available to runaway after the temperature drop. Higher Z_{eff} due to “killer” pellets gives a stronger hot-tail runaway effect. The parameter variations show that the hot-tail runaway process is a robust aspect of killer-pellet-induced electron runaway. Since plasma disruption gives a similar rapid temperature drop, the hot-tail runaway process must also be considered to accurately model disruption.

2 CQL3D Runaway Model

2.1 The Bounce-averaged FP Equation

CQL3D calculates a solution of the finite difference equations derived from the relativistic bounce-averaged (BA) Fokker-Planck (FP) equation, giving the time-evolution of the particle distribution $f_0(u_0, \theta_0, \rho t)$ in toroidally symmetric geometry. The distribution is evaluated at the point on a non-circular flux surface (labeled by ρ) where all particles pass, that is, at the minimum magnetic field equatorial plane point $\theta_{pol} = 0$, assuming up-down symmetry of the equilibrium. The (u_0, θ_0) -coordinates are electron momentum-per-rest-mass and pitch angle as measured from the magnetic field direction, at $\theta_{pol} = 0$. The electron distribution is taken to be azimuthally symmetric about the direction of the local B-field. The validity of the BA approximation is based on the assumption that the collision time is long compared to the bounce or transit time; this holds for present day hot tokamaks, in reactors, and also for sufficiently energetic tail particles in cooled plasma phases, as will be discussed at the end of this section. The distribution $f(u, \theta, \theta_{pol})$ at non-zero poloidal angle is equal, by the Liouville theorem, to the distribution at $\theta_{pol} = 0$, using the constants of collisionless motion which give (u, θ) as a function of poloidal angle,

$$u = u_0 \quad , \quad \frac{\sin^2 \theta}{B(\theta_{pol})} = \frac{\sin^2 \theta_0}{B(\theta_{pol} = 0)} \quad . \quad (1)$$

The BAFP equation is:

$$\frac{\partial(\lambda f_0)}{\partial t} = \frac{\partial}{\partial \mathbf{u}_0} \cdot \Gamma_{\mathbf{u}_0} + \lambda \langle \langle S \rangle \rangle \quad ; \quad (2)$$

$\Gamma_{\mathbf{u}_0}$ is the 2D momentum space flux due to bounce-averaging the effects of collisions, electric field, and additional slowing-down forces such as bremsstrahlung and synchrotron radiation. The quantity λf_0 is the number of particles per cross-sectional area on a field line with equatorial coordinates in $d^3 u_0$, where $\lambda \equiv v_{||0} \tau_B$, $v_{||0}$ is the particle parallel

velocity as it passes the equatorial plane, and τ_B is the bounce time:

$$\tau_B \equiv \oint d\tau_B = \oint \frac{dl_B}{|v_{\parallel}(u_0, \theta_0)|} . \quad (3)$$

Distance l_B is measured along the particle orbit from the equatorial plane. The quantity $\langle\langle S \rangle\rangle$ represents bounce-averaged sources and sinks, here due to the large angle knock-on source and due to stochastic magnetic field losses,

$$\langle\langle S \rangle\rangle \equiv 1/\tau_B \oint d\tau_B S(u(u_0, \theta_0)) \quad ; \quad (4)$$

the integrals are taken along a path which follow the collisionless particle motion taken in the present zero-banana width approximation to be exactly along the magnetic field lines.

An important point with respect to the collision operator is that it is nonlinear; the coefficients depend on the distribution itself and thereby momentum and energy conservation are maintained during a collision. Accounting for electron-electron momentum conservation during collisions is essential in order to accurately evaluate the electrical conductivity. Equation (2) is solved for each plasma radius ρ on a variable-spaced u_0, θ_0 -grid. The time-dependent differencing is fully implicit, and therefore time-steps are limited only on the basis that they must be sufficiently small to resolve the time scales of interest.

2.2 Radiation and Transport Loss Terms

Synchrotron radiation is accounted for by bounce-averaging the term given in [10],

$$\Gamma_{synchrotron} = \alpha |\mathbf{B}|^2 \gamma_{\perp}^2 \left\{ \hat{\mathbf{b}} \times (\mathbf{u} \times \hat{\mathbf{b}}) + \frac{|\hat{\mathbf{b}} \times \mathbf{u}|^2}{\gamma_{\perp}^2 c^2} (\hat{\mathbf{b}} \cdot \mathbf{u}) \hat{\mathbf{b}} \right\} f_e \quad , \quad (5)$$

where $\alpha = (2/3)[e^4/(m_e^3 c^5 \gamma)]$, $\gamma_{\perp}^2 \equiv 1 + u_{\perp}^2/c^2$, and $\hat{\mathbf{b}} \equiv \mathbf{B}/|\mathbf{B}|$. Bremsstrahlung is described by a slowing-down term [19]. We obtain $du/dt = -\beta u$ where $\beta = n_i c^2 \gamma \sigma_{rad}/u$, γ is the relativistic factor, and σ_{rad} is the cross-section given in the reference. Bounce-averaging these two radiation effects gives slowing-down contributions to the momentum-space flux Γ .

The magnetic flutter loss model used is [20]

$$\begin{aligned}\frac{\partial f_0}{\partial t} &= -\frac{f_0}{\tau_{\delta B}} \quad , \\ \tau_{\delta B} &= \frac{(\rho - a)^2}{4v_{\parallel} D_{st}} \gamma^5 \quad , \\ D_{st} &= \pi R_{\text{eff}} (\delta B_r / B)^2 \quad , \\ R_{\text{eff}}^{-1} &= (\pi q R)^{-1} + \lambda_{mfp}^{-1} \quad ,\end{aligned}$$

applied to the passing particles only. The mean free path is $\lambda_{mfp} = (u_{\parallel} / \gamma) / \nu_{\perp}^{ei}$, where a relativistic perpendicular collision frequency is used. Safety factor q has been taken to be 2. The γ^5 -factor follows the phase-averaging effect of electron orbits deviating from flux surfaces [21], although Ref. [22] finds this effect weakened. After each short time-step of the code, the electron distribution is renormalized to keep the electron density to a prescribed time-dependence.

2.3 Knock-on Collision Term

The “knock-on” collision source used in the code is obtained from the Moeller cross-section for large angle electron-electron collisions [23]. The usual collisional Fokker-Planck operator is valid for collisions which displace the electrons in velocity space by a small amount compared to the thermal velocity. These collisions are dominant for most purposes. However, in the calculation of the generation of runaway electrons, the relatively infrequent but large-velocity-increment collisions caused when very high velocity electrons have a close encounter with bulk electrons can greatly facilitate the production of runaway electrons. A “knock-on” collision of an energetic runaway electron hitting a bulk electron can impart enough momentum to the bulk electron to put it beyond the critical momentum-per-mass u_{crit} where the electric field acceleration exceeds the collisional slowing down,

$$u_{crit}/c = (E/E_0 - 1)^{-1/2} \quad ,$$

where $E_0 \equiv 4\pi n e^3 \ln(\Lambda)/(mc^2)$. This gives a regenerative (exponentially growing) source of runaway electrons, and will cause a runaway avalanche, given sufficient e-folding times and confinement of the runaways [5].

Denoting the pre-collision momenta-per-rest-mass by \mathbf{u}' for the thermal electrons and \mathbf{u}'_1 for the fast “primary” particles, and the post-collision momenta-per-mass by \mathbf{u} for the secondary “source” electrons and \mathbf{u}_1 for the slowed down primaries, then momentum and energy conservation may be written:

$$\begin{aligned}\mathbf{u}' + \mathbf{u}'_1 &= \mathbf{u} + \mathbf{u}_1 \\ E' + E'_1 &= E + E_1\end{aligned}$$

where $E \equiv (\gamma - 1)m_e c^2$, $\gamma^2 \equiv 1 + u^2/c^2$, and m_e is electron rest mass. We use the approximation that the pre-collision high energy tail electrons are colliding on zero-energy thermal particles (*i.e.*, $u' = E' = 0$). For the primary electrons, we also assume that their pre-collision momenta perpendicular to the magnetic field is zero ($u'_{\perp 1} = 0$), since parallel acceleration of the runaways is dominant. The secondary source electrons will then lie on an ellipse in momentum space,

$$\frac{u_{\perp}^2/c^2}{2(\gamma'_1 - 1)} + \left(\frac{u_{\parallel}}{u'_{\parallel 1}} - \frac{1}{2} \right)^2 = \frac{1}{4} \quad . \quad (6)$$

Figure 1(a) shows this source ellipse for several values of the primary momenta.

The “knock-on” source rate for source particles born in $d\gamma$, is denoted by ds . These particles are distributed along the ellipse, Eq. (6), and are a result of incident (primary) runaway electrons of density dn_r at momentum $u'_{\parallel 1}$ colliding with the bulk density n . We have

$$ds = n dn_r v_r \frac{d\sigma}{d\gamma} d\gamma \quad , \quad (7)$$

where $v_r = u'_{\parallel 1}/\gamma'_1$, $d\sigma/d\gamma$ is the Moeller cross-section ($d\phi/dq$ in the notation of Ref. [19]). In keeping with the approximation that the distribution of primary electrons has only parallel momenta, we obtain dn_r from the cold electron distribution according to

$$dn_r = \int^{\theta'} \sin\theta' d\theta' f(\mathbf{u}'_1) u_1'^2 du'_{\parallel 1} \quad , \quad (8)$$

where the θ' -integration covers the interval $[0, \pi/2]$ for positive $u'_{\parallel 1}$ and $[\pi/2, \pi]$ for negative $u'_{\parallel 1}$. We use the notation for the “parallel” distribution of electrons F

$$F(u'_{\parallel 1}) = \int^{\theta'} \sin\theta' d\theta' f(\mathbf{u}'_1) u_1'^2 \quad . \quad (9)$$

To obtain S , the source/(volume in momentum-space), we relate $d\gamma$ to du by $d\gamma = udu/(\gamma c^2)$, and $du'_{\parallel 1}$ to $\xi \equiv \cos\theta$. Thus, we have $du'_{\parallel 1} = \left. \frac{\partial u'_{\parallel 1}}{\partial \xi} \right|_u d\xi$; we use the pitch angle of the scattered particle from Heitler [23] to complete this calculation:

$$\xi^2 = \frac{(\gamma - 1)(\gamma'_1 + 1)}{(\gamma + 1)(\gamma'_1 - 1)} \implies \left. \frac{\partial u'_{\parallel 1}}{\partial \xi} \right|_u = \frac{\gamma'_1 u'_{\parallel 1}}{\xi} \quad . \quad (10)$$

We thus obtain the source S ,

$$S \equiv \frac{ds}{2\pi u^2 du d\xi} = nr_0^2 F(u'_{\parallel 1}) \frac{u_{\parallel 1}'^2}{\gamma \xi u c^2} \Sigma \quad , \quad (11)$$

where $r_0 = e^2/m_e c^2$ is the classical electron radius, and

$$\Sigma(\gamma, \gamma'_1) \equiv \frac{\gamma_1'^2}{(\gamma_1'^2 - 1)(\gamma - 1)^2(\gamma'_1 - \gamma)^2} \left\{ (\gamma'_1 - 1)^2 - \frac{(\gamma - 1)(\gamma'_1 - \gamma)}{\gamma_1'^2} [2\gamma_1'^2 + 2\gamma'_1 - 1 - (\gamma - 1)(\gamma'_1 - \gamma)] \right\} \quad .$$

For high energy runaways, $\gamma'_1 \gg 1$, we have $\Sigma \rightarrow 1/(\gamma - 1)^2$; consequently, Σ and the knock-on source $ds \propto \Sigma$ for given high energy primary electron density dn_r become independent of the energy of the primary runaway electrons. The secondary electron source strength ds is strongly peaked towards low energy and thus most of the contribution will come from the region near the runaway velocity boundary. From Fig. 1, the source will be highly localized in angle near the perpendicular direction.

We introduce a “cutoff” of the source at a point marginally below u_{crit} , in order to avoid “double counting” of collisional effects; the Fokker-Planck term accounts for small angle collision events which cause electron velocity changes less than the thermal velocity.

We also exclude source particles at energies higher than half the primary energy, and do not reduce the primary energy after a collision.

The above reduced distribution $F(u'_{\parallel 1}, l_B)$ and the source ds are formed locally in poloidal angle, specified here by l_B , the distance along B measured from the equatorial plane. Bounce averages of the knock-on source are then formed numerically according to the previous prescription Eq. (4). F is evaluated on the same u -grid as the equatorial plane distribution f_0 . We evaluate the distribution F of particles with momentum in du and in the interval dl_B at l_B in terms of the equatorial distribution computed in the code:

$$F(u, l_B) = 2\pi u_0^2 \psi(l_B) \int^{\theta_0} d\theta_0 \sin\theta_0 f_0(\mathbf{u}_0) |v_{\parallel 0}| d\tau_B / dl_B \quad . \quad (12)$$

(This relation can be derived by considering the flux of electrons into the interval dl_B , cross-sectional area d^2A , for time $d\tau_B$, and transforming back to equatorial plane coordinates using Eq. (1), and $f(\mathbf{u}, l_B) = f_0(\mathbf{u}_0)$, $Bd^2A = \text{const}$). The θ_0 -integration is carried out over the interval $[0, \theta_{0max}]$ for the positive-going electrons and $[\pi - \theta_{0max}, \pi]$ for the negative-going electrons. The quantity $\theta_{0max} = \theta_{0max}(l_B, \rho)$ is the maximum pitch angle at the equatorial plane of an electron which reaches l_B without bouncing. The ratio $\psi(l_B)$ is equal to B/B_0 . The quantity $d\tau_B$ for each dl_B on a l_B -grid is numerically calculated in the code. Density as a function of l_B , required for ds , is obtained by integrating F :

$$n(l_B) = \int_{-\infty}^{+\infty} du F(u, l_B) \quad .$$

The quantity ds is the pitch-angle integrated source in $d\gamma$. As can be seen from Fig. 1, a very narrow pitch angle region is sourced by a given group of runaway electrons $dn_r = F(u, l_B)du$. We therefore simply place the dn_r at the theta value given by the source ellipse, Eq. (6). Writing

$$\langle\langle S \rangle\rangle = (1/\tau_B) \oint d\tau_B \int ds / (2\pi u^2 du \sin\theta d\theta) \quad , \quad (13)$$

using Eq. (7) and (1), and $dl_B = |v_{\parallel}| \tau_B$ gives the bounce-averaged source evaluated in terms of the equatorial distribution,

$$\langle\langle S(u_0, \theta_0) \rangle\rangle = \frac{r_0^2 / \tau_B}{c^2 u_0^2 \sin\theta_0 \cos\theta_0 d\theta_0} \oint dl_B \frac{n_e(l_B)}{\psi(l_B)} \int_{-\infty}^{+\infty} du_{\parallel} F(u_{\parallel}, l_B) \frac{u'_{\parallel 1}}{\gamma_1} \Sigma(\gamma_0, \gamma_1) \quad . \quad (14)$$

The term $d\theta_0$ appears in the denominator, since we spread the source across this interval on the finite difference mesh in the code.

2.4 Accommodation for Non-banana-regime Conductivity

At the low temperatures occurring towards the end of the thermal quench, the plasma is no longer in the banana regime, and the bounce average results will be inaccurate for the low velocity portion of the electron distribution. To avoid exaggeration of the electrical field and unrealistic enhancement of calculated runaway production, the thermal portion of the electrical conductivity is calculated with a general neoclassical expression [17]. The portion of the electrical conductivity from runaway tail particles beyond the critical velocity u_{crit} is obtained from the Fokker-Planck calculations.

This procedure is justified in the usual case that the tail electrons beyond u_{crit} are in the banana regime. We examine this for thermal quench conditions in DIII-D. A typical current density profile is

$$j(\rho) = 150 \cdot [1 - (\rho/a)^2] \text{ amps/cm}^2 \quad . \quad (15)$$

Using Spitzer conductivity [24] with given (radially constant) density, temperature, and Z_{eff} , this specifies the toroidal electric field. We compare the resulting critical runaway velocity u_{crit} with the velocity u_{banana} above which electrons are in the banana regime, that is, for which their toroidal bounce frequency $\nu_{bounce} = \sqrt{\epsilon}(u/\gamma)/(qR_0)$ is greater than the collisional detrapping frequency $\nu_{eff} = \nu_{\perp}^{ei}/\epsilon$, where $\nu_{\perp}^{ei} = 4\pi n_e e^4 \ln\Lambda / [Z_{eff} \gamma^2 m_e^2 (u/\gamma)^3]$. Fig. 2. shows u_{crit} and u_{banana} versus radius, for (a) $n_e = 1 \cdot 10^{14} \text{ cm}^{-3}$ and (b) $2 \cdot 10^{14} \text{ cm}^{-3}$, $Z_{eff} = 4$, and several temperatures. The critical runaway velocity u_{crit} remains above the banana-regime cross-over velocity u_{banana} for the relevant conditions in DIII-D, validating our approach. It is observed that in a typical fusion reactor, since the current densities will also be approximately the same as in Eq. (16) and the other plasma conditions are also similar in the late quench period, then the neoclassical conductivity formulas must also be used for accurate calculation of bulk electrical conductivity .

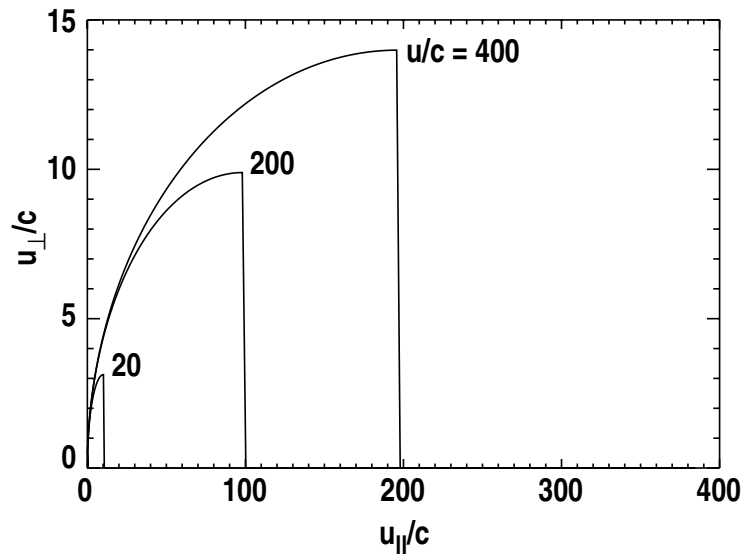


Fig. 1. Knock-on source ellipse. Primary electrons with parallel momentum as indicated on the curves impact low velocity electrons producing secondary source electrons with birth-points along the ellipses. The source strength is heavily weighted towards the lower velocities, in accord with Eqs~(11) and (12). The sources are cutoff at half the primary energy, keeping the distinction between primary and secondary particles.

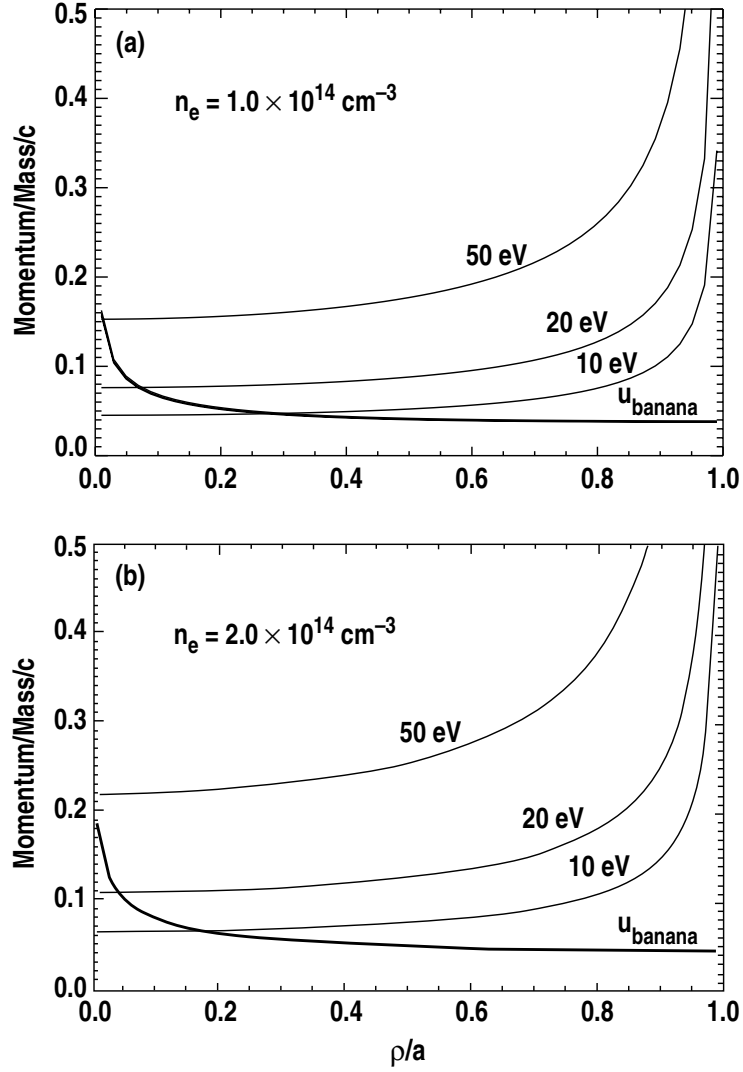


Fig. 2. Momenta-per-mass versus plasma radius, above which the banana regime is valid in DIII-D geometry is shown in the curve labelled u_{banana} . The curves marked by 10, 20, and 30-eV are the values of runaway velocity u_{crit} obtained for a current density of 150 $[1 - (\rho/a)^2]$, at the indicated temperatures, with plasma density (a) $1 \cdot 10^{14} \text{ cm}^{-3}$, and (b) $2 \cdot 10^{14} \text{ cm}^{-3}$. $Z_{\text{eff}}=1$ is assumed. For $u_{\text{crit}} > u_{\text{banana}}$, the electrons are in the banana regime.

3 Runaway Production During Ne Pellet Injection

In this section, results are presented for the evolution of the electron distribution as the temperature, density, and Z_{eff} evolve due to Ne pellet injection during a particular DIII-D shot (#88806). The background plasma parameter evolution is calculated with the KPRAD code [15], and the kinetic evolution of the electron distribution with the CQL3D code.

A pellet ablation model is used with KPRAD to calculate the pellet plasma source. At each radius, the time-evolution is calculated for four plasma populations: initial plasma electrons and ions, impurity ions from the pellet, and electrons arising from ionization of the impurities. The charge state balance is calculated from ionization and recombination rates. Energy balance for each species and their various ionization states includes using the ADPAK rate coefficients to compute the radiation effects, and the Spitzer conductivity to compute Joule heating and the toroidal electric field. The species are collisionally coupled via Coulomb collisions. Radial heat transport is neglected during the short time of the thermal quench. Figure 3 shows calculated temperature, density, and Z_{eff} evolution at the typical radius $\rho = 0.6a$, versus time measured from the arrival of the pellet at the flux surface. Current density is 75 Amps/cm². The thermal quench occurs in 100 μ s. In DIII-D, this pellet scenario is marginal for the production of runaway electrons. Variations around this scenario are presented in the next section.

Figure 4 gives the evolution of the electron distribution calculated with CQL3D as the plasma evolves during the 100 μ s period of the pellet-induced temperature drop and density increase. The density in the distribution is evolved in accord with KPRAD, Fig. 3(b), by adding density with a Maxwellian temperature in accord with Fig. 3(a). The solution for this distribution function is fully nonlinear in that the electrons self-collide on a distribution obtained by fitting Legendre polynomials to the distribution in the manner of Ref. [12], *except* that the P_0 -expansion term is a Maxwellian density and temperature to fit the KPRAD specified values. This approach models effects of transport which operate

primarily on the bulk electrons. It is a good approximation when the tail electrons are dominated by collisions rather than transport, except for the effect of the explicitly specified stochastic magnetic field term. Losses due to magnetic field fluctuations with $\delta B_r/B = 0.001$ are included. The background ion Z_{eff} is also varied, as in Fig. 3(c). Cuts of f_0 versus u , at several fixed pitch angles θ_0 are shown in Fig. 4. Below each of the distribution functions, the “specific current density” $j'(u)$ is shown

$$j'(u) = \int d\theta_0 2\pi \sin\theta_0 (u_{\parallel}/\gamma_0) u_0^2 f_0(\mathbf{u}_0) \quad ,$$

such that the current density due to electrons is $j = -e \int_0^\infty du j'(u)$.

Figure 4(a) shows the 2.2 keV distribution function immediately before the pellet effects. This distribution carries the 75 Amps/cm² current distributed as shown by $j'(u)$, where $j'(u)$ is the usual velocity distribution of Ohmic current peaked near $2.5v_{te}$. In the Fig. 4 plots, only a portion of the momentum mesh, up to $0.5c$ is shown; the calculation is performed on a mesh which extends to $200c$ (100 MeV) and electrons are stopped before leaving the mesh by an artificially large Bremsstrahlung-like slowing down term applied near the maximum momenta on the mesh. After 0.05 ms the distribution has evolved into a core portion in equilibrium with the 30 eV background temperature shown in Fig. 4(b). The electric field has increased in accord with the assumed constant current density giving $u_{\text{crit}}/c = 0.13$; at this point in time the runaway portion of the distribution, determined by integrating $j'(u)$ beyond u_{crit} , encompasses 60 percent of the total current. The steady-state knock-on growth rate [4] is 450 s^{-1} , and, thus, this source of electrons is not important on this short time scale. Since $E/E_{\text{Dreicer}} = 0.007$, the Dreicer runaway effects are negligible, *cf.* Ref. [25]. After evolution for a further 0.05 ms, Fig. 4(c) at $t = 0.1 \text{ ms}$ shows the near steady-state distribution. The knock-on growth rate is 600 s^{-1} , and the Dreicer runaway rate remains extremely small. Although the $j'(u)$ -plot shows a substantial portion of the plasma current carried by the thermal particles below $0.03c$, the higher velocity portion (beyond what is shown) integrates to 0.2 of the total plasma

current. Thus, a large *hot-tail runaway* distribution has been formed in 0.1 ms by direct transfer of a portion of pre-pellet hot electron tail distribution to runaways.

Figure 5 clarifies further the dynamics of the hot-tail runaway effect. The fractional (a) runaway density and (b) runaway current jump to high value and then fall back to sustainable values in the time scale of 0.1 ms. The transport loss time $\tau_{\delta B}$ is approximately 0.2 ms at $u/c = 0.1$ and it is this effect which pulls the runaway fraction down. By comparison, a no-loss run gives a steady $j_{run}/j_0 = 1.0$ in 0.1 ms. Both (c) the electric field E and (d) the knock-on source rate quickly approach quasi-steady values, with E/E_0 a large value (in this case ≈ 500) rather than asymptotically 1.0 as in the no-loss case [6].

The effect of knock-on electron production becomes evident at longer times, as shown in Fig. 6 which gives results from a simulation (a) with the knock-on source, and (b) without it. In the absence of knock-on replenishment of the tail electrons (b), the electrons sourced by the hot-tail runaway are lost and the runaway current dies.

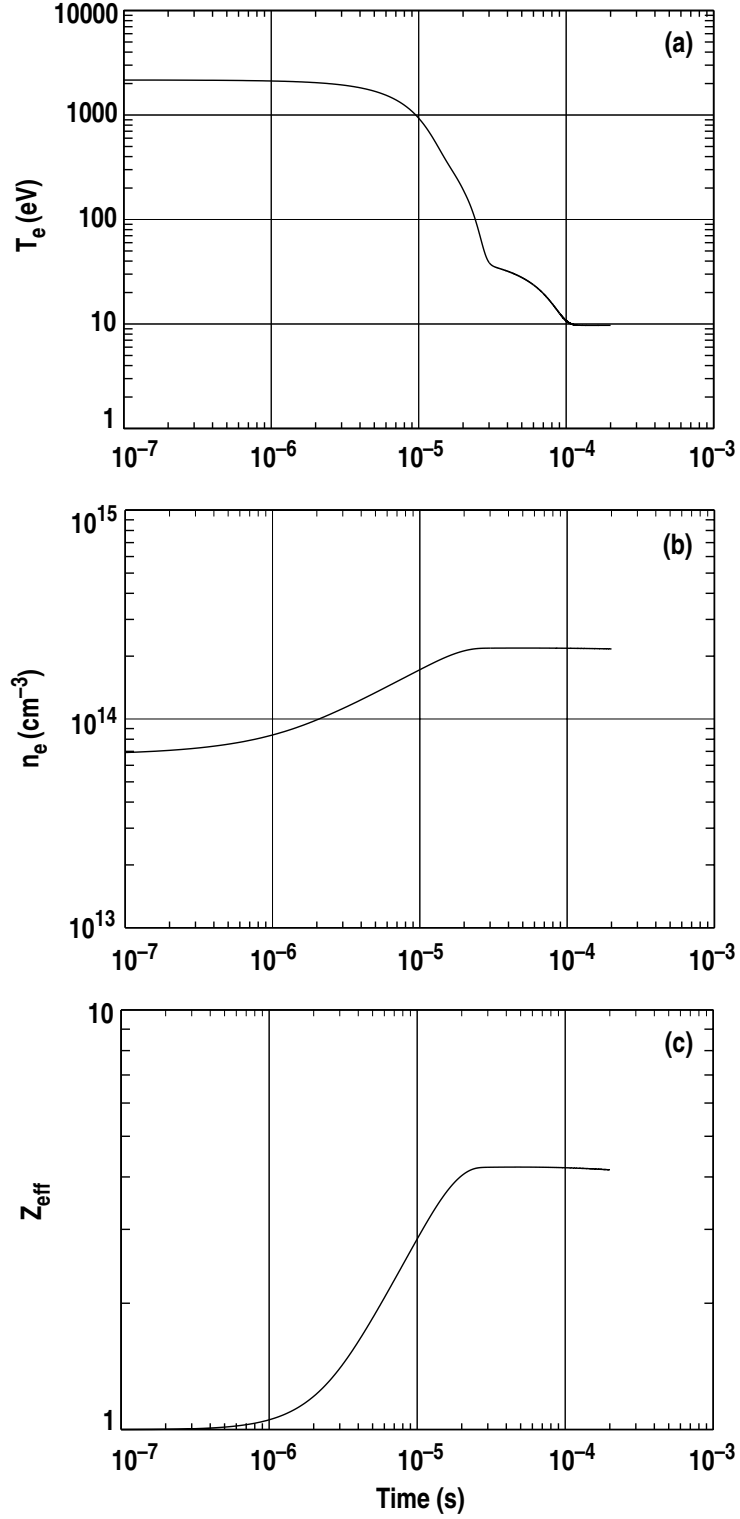


Fig. 3. The time-variation of (a) electron temperature, (b) plasma density, and (c) Z_{eff} obtained by the KPRAD radiation code at plasma radius $\rho = 0.6a$, modeling a Ne pellet injection into DIII-D shot 88806. Time is measured starting at the moment the pellet reaches the flux surface.

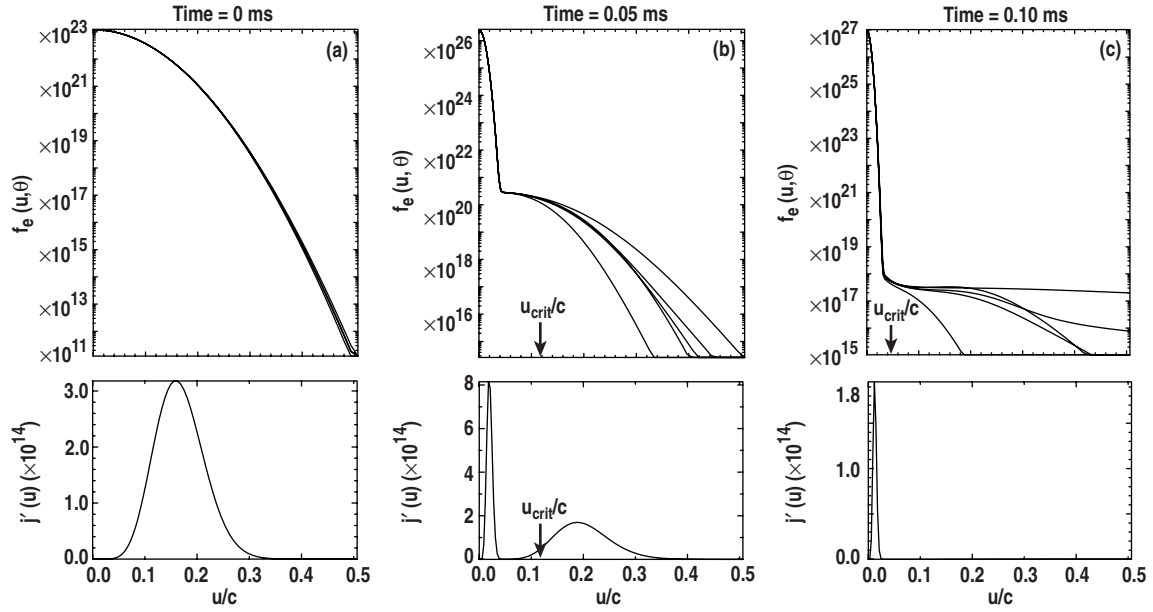


Fig. 4. Calculated 2D-in-momentum-space electron distributions at times (a) $t=0$ ms, (b) $t=0.05$ ms, and (c) $t=0.10$ ms, using the background plasma variations in Fig. 3. The upper plot in each pair show cuts through the distribution function versus momentum-per-rest-mass u_0 , at constant pitch angles θ_0 corresponding to directions parallel to the magnetic field, at the trapped-passing boundary, perpendicular, and anti-parallel, and a pitch angle averaged distribution. The highest tail curve corresponds to the electric field drift direction, and the lowest to the counter-drift direction. Values of u_{crit} are marked on the horizontal axis. The lower plot in each pair shows the momentum distribution $j'(u)$ of the current. Only a portion of the computational mesh up to $u = 0.5c$ is shown. A large prompt runaway electron tail is formed in 0.10 ms.

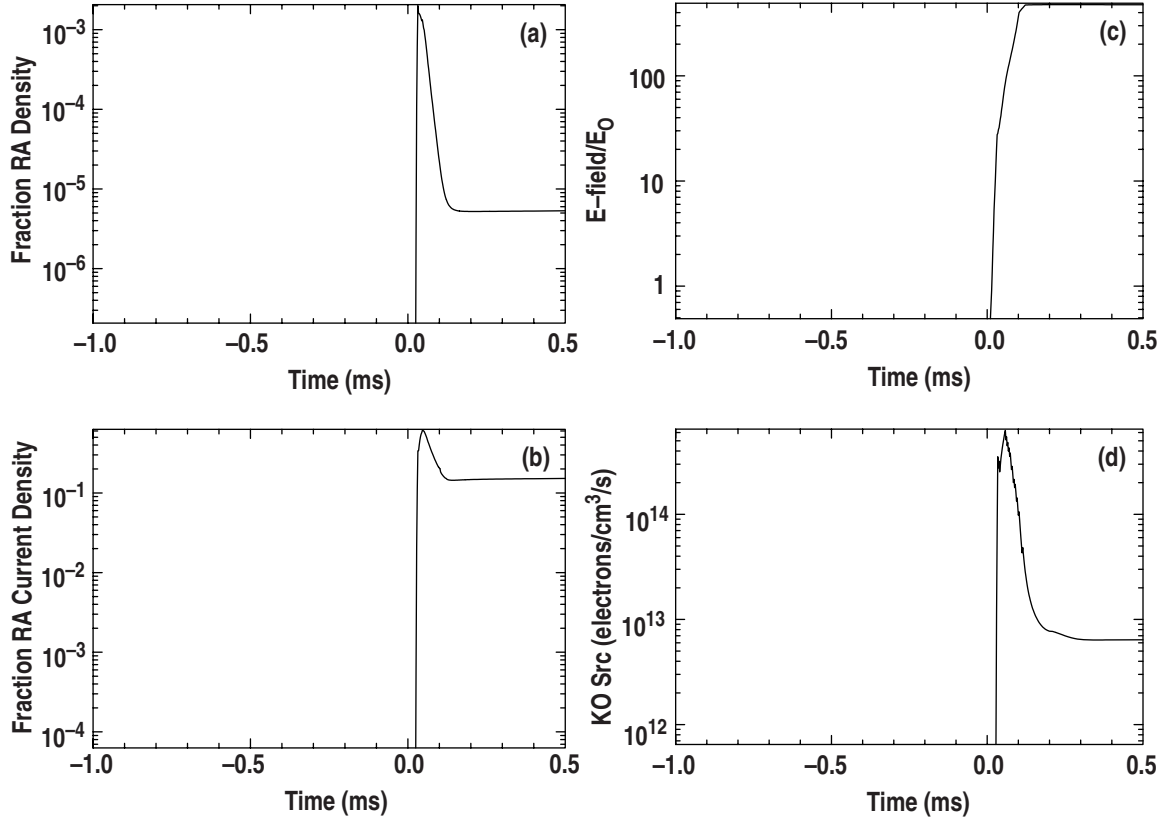


Fig. 5. Time-evolution of quantities derived from the kinetic modeling: (a) fractional runaway density, (b) fractional runaway current, (c) ratio of electric field to critical electric field, and (d) the knock-on source rate of secondary electrons born above the runaway velocity u_{crit} . The level of stochastic magnetic field losses is given by $\delta B_r/B = 0.1\%$.

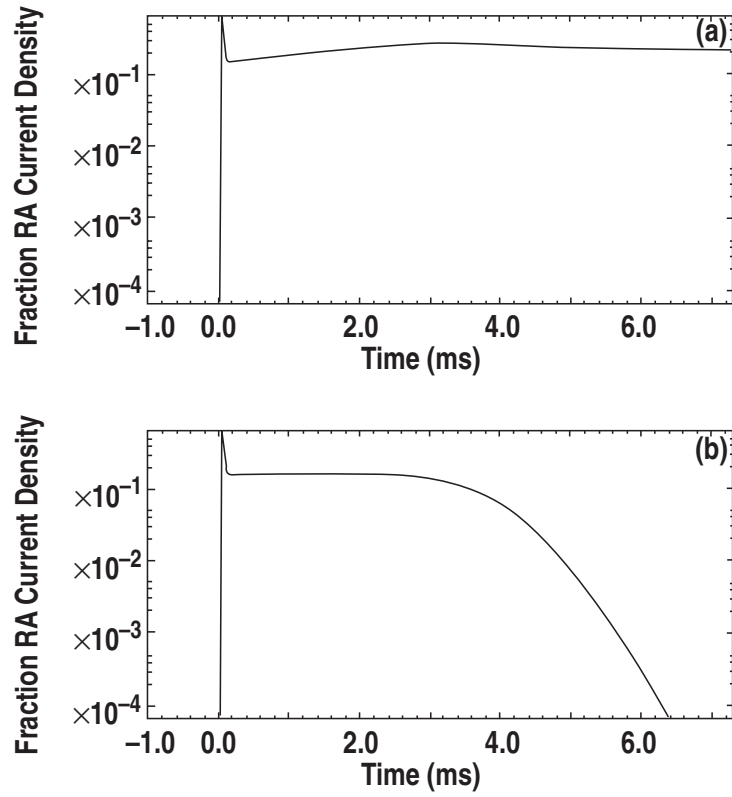


Fig. 6. Comparison of the time-evolution of the runaway current fraction obtained in our baseline case with $d B_r/B = 0.1\%$ with (a) the knock-on operator turned on, and (b) the unphysical case of knock-on operator turned off. It is evident that while the prompt hot-tail runaways provide the major source of runaway current at short times, the knock-on source provides the source which sustains the runaway current.

4 Variation of Parameters of the Simulation

The previous section showed the possible importance of the *hot-tail runaway* process in a DIII-D pellet experiment. In this section, parameters of the above run will be varied in order to determine the robustness of the phenomena and to enable extrapolation of the results to other experimental situations. The magnetic fluctuation level (*i.e.*, losses), density, Z_{eff} , and the temperature drop time-scale have been varied.

The steady-state runaway current fraction is a sensitive function of magnetic losses (Fig. 7). Magnetic fluctuation losses applied at $\rho/a = 0.6$ with $\delta B_r/B = 0.1\%$ give runaway current fraction of 0.2. If $\delta B_r/B$ is increased by 40 percent the runaways are eliminated, whereas if $\delta B_r/B$ is decreased by 50 percent the current is 100 percent runaways. This effect appears even sharper for $\rho/a = 0.9$; in which case, the runaway current is completely eliminated for $\delta B_r/B \geq 0.02\%$.

These results are in general accord with the estimates of $\delta B_r/B$ levels which eliminate killer-pellet generated runaway current in DIII-D [26]. Experiments performed on JT-60U with applied radial magnetic perturbations $\delta B_r/B$ in excess of 0.12% suppressed runaway electron generation during discharge terminating disruptions [27]. This result is also in accord with the present calculations.

It has been proposed to create larger density increases than used in the present killer-pellet experiments in order to decrease the conversion of plasma current to runaway current [28]. This has been modeled by varying the time-dependence of the density used in the previous section. The density dependence in Fig. 3(b) was fitted by a relation linear in $\log(n_e)$ versus $\log(t)$, between the initial and final density values in the time interval $1 - 20 \mu\text{s}$; the time-dependence was then varied by changing the final density. Magnetic fluctuation losses were turned off for this modeling. We plot fractional runaway densities versus final density, since fractional values in excess of 10^{-8} are important as seed populations for the knock-on avalanche process. Figure 8 shows a log-linear reduction in the fractional runaway density as the final plasma density is increased. Also marked

along the curve is the fraction of prompt runaway current due to the hot-tail effect. Since there are no losses, the knock-on runaway source eventually brings all these cases to 100% runaway conversion. The conclusion from this figure is that the hot-tail runaway electrons are an important effect in the dynamics of runaway formation for densities below 10^{15} cm^{-3} . They lead to prompt runaway conversion or provide the major seed population for the knock-on avalanche.

The logarithmic decrease in the fraction of runaway electrons can be explained as follows: the electric field $E(t)$ variation depends on plasma conductivity and is therefore independent of the plasma density. The hot-tail electrons decrease in time $\propto \exp(-t/\tau_{slow})$, where the electron slowing down time τ_{slow} is $\propto n_e^{-1}$. Thus we have $n_{run}/n_e \propto \exp(-constant \cdot n_e)$, in accord with the above simulations.

Varying the final Z_{eff} in a manner analogous to the above density variation gives prompt runaway density fractions as shown in Fig. 9. (We refer to Fig. 5(a) showing an initial large prompt runaway density fraction as given in Fig. 9; the runaway density fraction then tapers off in a fraction of a ms due to the decreasing conductivity which gives reduced electric field.) The variation of density and temperature are the same as in Fig. 3, and the losses are turned off. The larger final values of Z_{eff} result in increased prompt runaway density fraction: Thus, $E(t)$ will increase with Z_{eff} due to the increased conductivity. This reduces $u_{crit} \propto E^{-1/2}$ which gives a larger hot runaway tail.

Finally, the time-scale for the temperature drop has been varied around the Fig. 3(a) dependence. This is done by fitting a linear in $\log(T_e)$ versus $\log(t)$ dependence from the initial to final temperature in Fig. 3(a), for the interval from $t = 5 \mu\text{s}$ to $t = 0.1 \text{ ms}$. The time of final temperature is then varied, giving various T_e -decrease times τ_{T_e} . Figure 10 shows runaway current conversion versus $\delta B_r/B$ transport loss level, with τ_{T_e} as parameter. The value $\tau_{T_e} = 100 \mu\text{s}$ corresponds to the previous section simulation. For zero or small $\delta B_r/B$, there is 100% conversion of plasma to runaway current for a wide range of temperature drop time τ_{T_e} , up to at least 1 ms, although the time interval for conversion

(not shown) strongly increases with τ_{T_e} . As τ_{T_e} decreases, the amount of $\delta B_r/B$ necessary to suppress runaway conversion increases. This final result is in general accord with the DIII-D experiment, for which Argon pellets lead to shorter τ_{T_e} and substantially greater runaway currents [15, 18, 26].

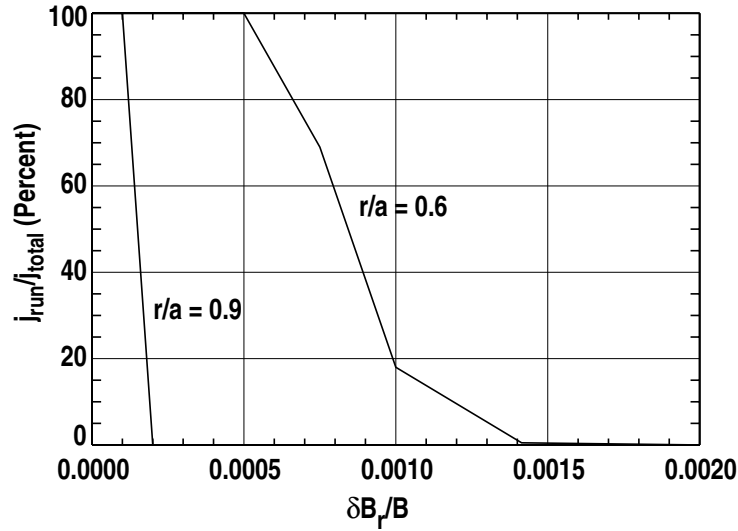


Fig. 7. Runaway current fraction versus loss parameter $\delta B_r/B$, for two plasma radii. With no losses the runaway current fraction is essentially 100 percent, but losses reduce the conversion of plasma current to runaway current in general accord with experimental observations. The $\delta B_r/B$ -losses are more effective towards the plasma edge because of the nearness of the loss boundary.

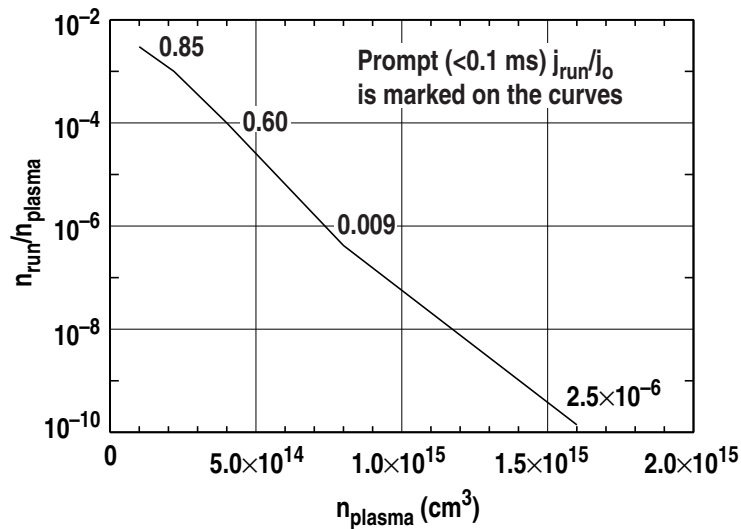


Fig. 8. Runaway density fraction versus final density achieved by the pellet injection. The prompt fraction of runaway current is marked along the curve. Losses are turned off. At the lower final densities, the prompt runaway fraction is almost unity and the simulation shows rapid growth to full runaway current due to the knock-on source. At higher final density up to $\sim 1.5 \cdot 10^{15} \text{ cm}^{-3}$, the prompt runaway electron will provide the major seed population for the knock-on ramp up of the runaway current

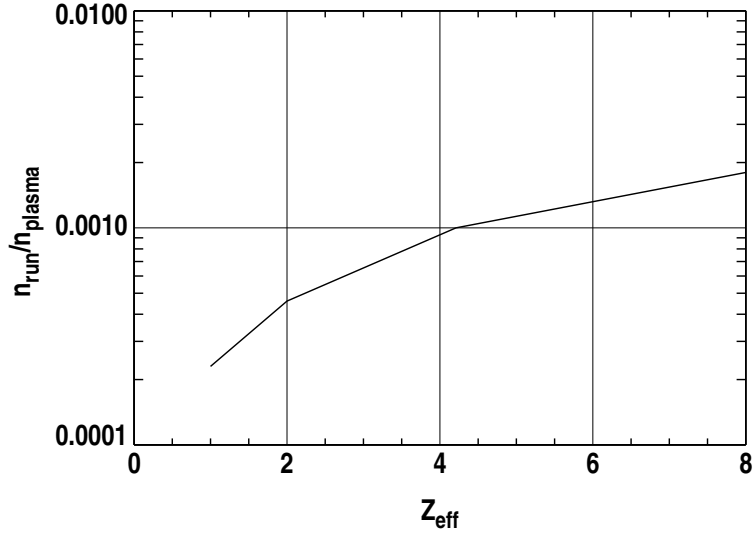


Fig. 9. Prompt “hot tail” runaway density fraction versus final Z_{eff} due to the pellet, with no losses, $\rho/a = 0.6$.

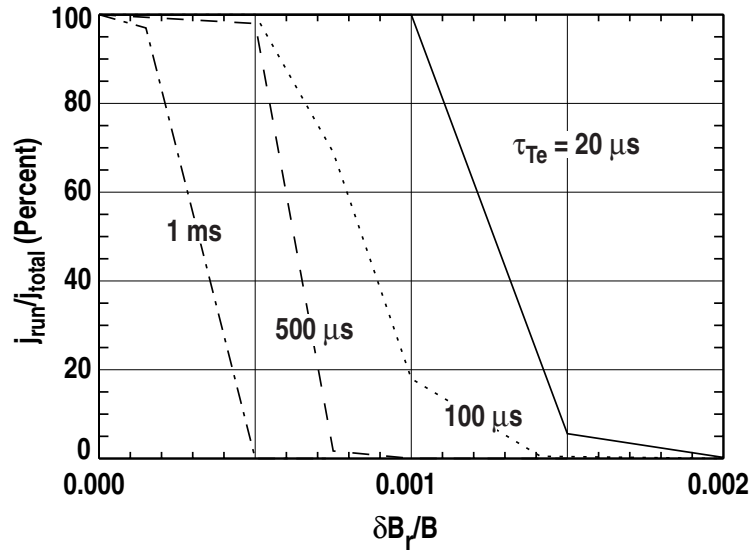


Fig. 10. Fractional runaway current versus $\delta B_r/B$, with the temperature-drop-time τ_{T_e} as a parameter. Plasma radius is $r/a = 0.6$. The $\delta B_r/B$ -losses can reduce the conversion of plasma current to runaway current to zero; as τ_{T_e} decreases, larger $\delta B_r/B$ is required to suppress the current conversion.

5 Conclusions

CQL3D/KPRAD modeling shows the possibility in DIII-D killer pellet experiments for prompt complete conversion of plasma current to runaway electron current by the *hot-tail runaway* mechanism, *i.e.*, runaway of the residual high energy electrons remaining after a rapid plasma temperature drop. With no losses, the *hot-tail runaway* process dominates knock-on and “Dreicer drizzle” formation of runaways, giving full prompt conversion of the plasma current to runaway current. Variations around the KPRAD model of n_e , T_e and Z_{eff} time dependence show that the *hot-tail runaway* effect is robust. For pellet induced density increases in DIII-D up to $\approx 1 \cdot 10^{15} \text{ cm}^{-3}$ (five times the experimental values) the hot-tail runaways dominate the early post-pellet evolution and provide the major seed population for late-time knock-on runaway avalanche. Lengthening the plasma cooling time due to the killer pellet to a factor of five greater than that calculated by the radiation code shows, in the absence of losses, a prompt conversion to runaway current of 0.2 of the plasma current by the hot-tail runaway mechanism, then rapid knock-on avalanche to full conversion in 1 ms.

A stochastic field loss model in CQL3D shows that the buildup of runaways can be suppressed by magnetic field perturbations with $\delta B_r/B \geq 0.1\%$, in general agreement with inferred $\delta B_r/B$ observations in DIII-D (and JT-60U). With losses included, knock-on collisions become essential to sustaining a level of runaway electrons. The value of the electric field asymptotes in time to a large value, 500 in our modeling for $\delta B_r/B = 0.1\%$, rather than to 1 in cases with no losses. Recent studies of the effects of magnetic fluctuations also find $\delta B_r/B \geq 0.1\%$ suppresses runaway avalanche [29, 30].

References

- [1] R. Jayakumar, H.H. Fleischmann, and H.H. Zweben, *Phys. Lett. A* **172**, 447 (1993);
H.H. Fleischmann and S.J. Zweben, “Evaluation of potential runaway generation in large-tokamak disruptions,” Princeton Plasma Physics Laboratory Report PPPL-2914 (June, 1993).
- [2] R. Jaspers, N.J. Lopez Cardozo, F.C. Schüller, K.H. Finken, *et al.*, *Nucl. Fusion* **36**, 367 (1996).
- [3] S.V. Putvinski, N. Fijisawa, D. Post, N. Putvinskaya, *et al.*, *J. Nucl. Mater.* **241**, 316 (1997).
- [4] S.C. Chiu, M.N. Rosenbluth, R.W. Harvey, V.S. Chan, *Nucl. Fusion* **38**, 1711 (1998).
- [5] Yu.A. Sokolov, *JETP Lett.* **29**, 244 (1979).
- [6] M.N. Rosenbluth and S.V. Putvinski, *Nucl. Fusion* **37**, 1355 (1997).
- [7] H. Dreicer, *Phys. Rev.* **115**, 23 (1959) and **117**, 329 (1960).
- [8] R.W. Harvey and M.G. McCoy, “The CQL3D Fokker-Planck Code,” Proc. of IAEA Technical Committee Meeting on Advances in Simulation and Modeling of Thermonuclear Plasmas, Montreal, Canada, 1992, (International Atomic Energy Agency, Vienna, 1993) pp. 489-526.
- [9] G.D. Kerbel and M.G. McCoy, *Phys. Fluids* **28**, 3629 (1985).
- [10] I.B. Bernstein, and D.C. Baxter, *Phys. Fluids* **24**, 108 (1981).
- [11] M. Franz, Lawrence Livermore National Laboratory Report UCRL-96510 (1987).
- [12] M.N. Rosenbluth, W.M. MacDonald, and D.L. Judd, *Phys. Rev.* **107**, 1 (1957).

- [13] T.E. Evans, A.G. Kellman, D.A. Humphreys, M.J. Schaffer, *et al.*, J. Nucl. Mater. **241-243**, 606 (1997).
- [14] R. Yoshino, T. Kondoh, Y. Neyatani, K. Itami, and N. Isei, Plasma Phys. Contr. Fusion **39**, 313 (1997); R. Yoshino, S. Tokuda, Y. Kawano, Nucl. Fusion **39**, 151 (1999).
- [15] D.G. Whyte, T.E. Evans, A.G. Kellman, D.A. Humphreys, *et al.*, Proc. of the 24th Euro. Conf. on Controlled Fusion and Plasma Physics, Berchtesgaden, Germany, 1997, Vol. 21A, p. 1137.
- [16] H. Fleischman, personal communication (1997).
- [17] F. Hinton and R. Hazeltine, Rev. Mod. Phys. **48**, 239 (1976).
- [18] P.L. Taylor, Phys. Plasmas **6**, 1872 (1999).
- [19] *Physics Vade Mecum*, Edited by H.L. Anderson, Second edition, Sec. 16.07.F, American Institute of Physics, New York (1989).
- [20] A.B. Rechester and M.N. Rosenbluth, Phys. Rev. Lett. **40**, 38 (1978); R.W. Harvey, M.G. McCoy, J.Y. Hsu, and A.A. Mirin, Phys. Rev. Lett. **47**, 102 (1981).
- [21] H.E. Mynick and J.D. Strachan, Phys. Fluids **24**, 695 (1981).
- [22] S. Tokuda and R. Yoshino, Nucl. Fusion **39**, 1123 (1999).
- [23] W. Heitler, *The Quantum Theory of Radiation*, Third edition, Dover Publications, New York, 1953, p. 240.
- [24] L. Spitzer and R. Härm, Phys. Rev. **89**, 977 (1963).
- [25] R.M. Kulsrud, Y-C. Sun, N.K. Winsor, and H.A. Fallon, Phys. Rev. Lett. **31**, 690 (1973).

- [26] T.E. Evans, P.L. Taylor, A.G. Kellman, P.B. Parks, *et al.*, Proc. IAEA Meeting, Yokohama 1998, Vol. 3, p. 847.
- [27] Y. Kawano, R. Yoshino, Y. Neyatani, T. Kondoh, N. Isei, *et al.*, Proc. of the 24th Euro. Conf. on Controlled Fusion and Plasma Physics, Berchtesgaden, Germany, 1997, Vol. 21A, Part II, p. 501.
- [28] M.N. Rosenbluth, S.V. Putvinski, and P.B. Parks, Nucl. Fusion **37**, 955(1997); P.B. Parks, M.N. Rosenbluth, S.V. Putvinski, and T.E. Evans, Fusion Technology **35**, 267 (1999).
- [29] J.R. Martín-Solís, R. Sáñez, B. Esposito, to be published in Phys. Plasmas (200).
- [30] P. Helander, L.-G. Eriksson, and F. Andersson, EURATOM/UKAEA Fusion Report UKAEA FUS 427, Culham Science Centre, Abingdon, United Kingdom (2000).

6 Acknowledgments

This research was supported by the U.S. Department of Energy under Contracts DE-AC03-99ER54463 and DE-FG03-99ER54541. R.W. Harvey gratefully acknowledges conversations with Dr. P.B. Parks, useful to this work, and very helpful review by Dr. P.L. Taylor.